ACS OMEGA

Open Access

http://pubs.acs.org/journal/acsodf

Article

Electric Field-Assisted Molecularly Imprinted Polymer-Modified QCM Sensor for Enhanced Detection of Immunoglobulin

Iliya LariMojarad, MirBehrad Mousavi, Mohammad Mahdi Moeini Manesh, Mohammadjavad Bouloorchi Tabalvandani, and Majid Badieirostami*

Cite This: *ACS Omega* 2024, 9, 16026−16034

Read Online

ACCESS | Metrics & More | Article Recommendations

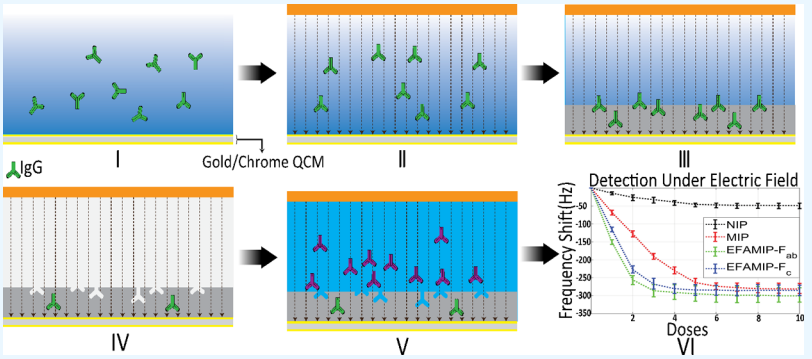

ABSTRACT: In this study, an electric-field-assisted molecularly imprinted polymer (EFAMIP) as an enhanced form of MIP was developed to improve the MIP-modified quartz crystal microbalance (QCM) biosensors. While exerting a vertical electric field, polymerization of methacrylic acid in the presence of immunoglobulin G (IgG) as the template was initiated, and later, after the template removal process, the EFAMIPs were obtained. The polymer surface characterization was conducted by using a scanning electron microscope. The impact of electric field direction on IgG binding sites, forming either EFAMIP-F_{ab} or EFAMIP-F_c, was assessed. Next, the static measurement results in liquid for EFAMIP-modified QCM and MIP-modified QCM were compared. While encompassing IgG, EFAMIP-modified QCMs exhibited up to a 113.5% higher frequency shift than typical MIP in time-limited detection. The final frequency shift of EFAMIP, which determines the detection limit of IgG, was improved up to 12.5% compared to typical MIP. Moreover, the EFAMIP-F_{ab} performance was promising for the selective detection of IgG in a solution containing different types of immunoglobulins.

1. INTRODUCTION

Biosensors are ingenious and innovative devices that have facilitated humans' well-being substantially. These analytical tools can detect a variety of biomarkers in real time, making them useful in a diverse range of applications, such as healthcare,[1,2] point-of-care (PoC) diagnostics,[3,4] and environmental monitoring.[5] They have especially revolutionized how diseases are diagnosed and treated, allowing for earlier detection and more precise treatment, with the ultimate goal of lowering the cost of healthcare and enabling personalized medicine.[6,7]

Antibodies are large Y-shaped proteins that the immune system recruits to identify and neutralize foreign harmful objects like pathogens, toxins, and chemicals.[8,9] A foreign substance that can bind to an antibody is called an antigen.[10] A specific antibody can bind with a particular antigen and protect the body from foreign molecules.[11] Thus, the presence of antibodies is crucial for the good performance of the immune system. If a specific antibody is deficient in one's body, one is likely not entirely immune or yet has not been exposed to the complement antigen.[12] In other words, if a specific antibody exists in one's body, they are assumed to be less prone to suffer from the corresponding antigen. This makes the measurement of the antibody ratio in blood vital. Among the most common antibodies in human blood is immunoglobulin (IgG) that can neutralize toxins, activate the complement system, and show current infections.[13] Therefore, the accurate measurement of IgG in blood is something significant.[14]

Molecularly imprinted polymers (MIPs) are synthetic receptors that emulate the recognition properties of their

Received: November 29, 2023
Revised: February 24, 2024
Accepted: March 13, 2024
Published: March 29, 2024

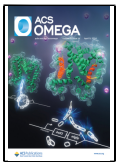

target molecules.[15] MIPs are synthesized by performing a polymerization reaction in the presence of target molecules, which serve as templates.[16,17] The monomers congregate around the target molecules; consequently, the polymerization reaction produces a structure around the templates.[18] Removing the templates from the polymer matrix leaves recognition cavities complementary to the target molecules in terms of shape and position of the functional bodies.[19] Thus, the target molecules can selectively bind to the cavities created in MIPs via a combination of noncovalent interactions.[20−22] The main challenges that MIPs face are as follows: achieving the levels of target specificity comparable to those of antibody−antigen biosensors, accurately detecting the presence of target molecules in a short period of time, dealing with the partial removal of templates during the elution step, and handling the entrapment of antibodies beneath the surface of the polymer.[23]

Quartz crystal microbalances (QCMs) are the basis of economic and reproducible biosensors, mainly consisting of a thin quartz crystal disk sandwiched between two electrodes oscillating at a specific frequency that alters when the resonator mass changes.[24,25] When the quartz disk surface is functionalized with MIPs, a selective biosensor is achieved, which is capable of measuring the existence of a specific antibody.[26−30] A simplified model for the working principle of the MIP-modified QCM is as follows. The prepolymerized solution membranes (mixture of monomer, cross-linker, and template molecules) are polymerized on the QCM, and then the template molecules are removed in a process called template removal. At this point, cavities are similar to template molecules formed on MIP-modified QCM. Throughout the detecting phase, a solution containing the target molecules is introduced to the system. Target molecules start to fill the cavities, and their mass becomes attached to the MIP-modified QCM. As the attached mass increases, the oscillation frequency of the QCM drops. Therefore, the presence of target molecules in a sample can be determined. Keep in mind that similar molecules can attach to the MIP cavities, culminating in an inaccurate frequency shift of QCM; this undesirable attachment is called nonselective adsorption, which we have discussed in the following sections. Eq 1 describes how the QCM's frequency shift relates to the change in mass accumulated on its surface.[24,31,32] Δf_r stands for the frequency shift, while f_0 is the initial oscillating frequency, Δm is the change in mass (g), A is the effective area (cm^2), ρ_q is quartz density ($g\ cm^{-3}$), and μ_q stands for quartz shear modulus ($g\ cm^{-1}\ s^{-2}$). It is worth mentioning that this equation is just valid for a thin rigid layer of mass change.[24,33] However, many studies in this field focused on fabricating a microfluidic setup that makes the commercial and user-friendly usage of MIP-modified QCM an arduous task.[34,35] In order to alleviate the use of MIP-modified QCM sensors, static measurements in the liquid phase were conducted as an alternative to the traditional ways. Eq 2 replaces eq 1, where the viscosity and density of the Newtonian solution also play roles in the frequency shift.

$$\Delta f_r = -\frac{2f_0^2 \Delta m}{A\sqrt{\rho_q \mu_q}} \quad (1)$$

$$\Delta f_r = -f_0^{3/2}\sqrt{\frac{\rho_l \eta_l}{\pi \rho_q \mu_q}} \quad (2)$$

As mentioned earlier, antibodies can be resembled with a Y-shaped structure; Figure 1 shows a typical antibody with its

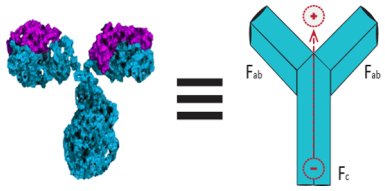

Figure 1. IgG dipole-like characteristic

two fragments, namely, F_{ab} and F_c. This structure can be modeled with an electric dipole in an intermediary buffer pH level condition, since the F_c fragment is negatively charged and the F_{ab} fragment is positively charged.[36−38] Therefore, by applying an electric field to antibodies, they all will be reoriented and consequently aligned identically along the same direction.[38−40] This remarkable characteristic of antibodies can be utilized to address the challenges listed for MIP-modified QCMs. In this paper, the effect of the exertion of an electric field on antibodies is assessed. The electric field will tilt the antibody dipole-like templates to create a similar pattern on the MIP surface. Later, by removing the antibody templates, the remaining cavities mostly have orientations specific to those of the antibody templates. The end result of this process is recognized as an electric field-assisted molecularly imprinted polymer (EFAMIP). Now, with regard to the sensing phase in the presence of the target, i.e., IgG, the sensitivity and recognition time are extremely enhanced by applying a similar electric field to antibodies, matching them with the cavities embedded into the EFAMIP surface. Consequently, this enables a more precise measurement of the antibody's ratio in the solution, which manifests itself in the frequency shift of QCM.

Following on in this paper, methacrylic acid (MAA) was utilized as the monomer while applying the vertical electric field (both the upward and downward electric field directions have been considered) and through bulk polymerization in the presence of ethylene glycol dimethacrylate (EGDMA) as a cross-linker and IgG as the template; poly(methacrylic acid) (PMAA) was made on the QCM surface. Studies have indicated that selectivity is directly proportional to material stiffness, which reinforces the importance of finding the proper rigidity.[41] The nature of the cross-linker and its primal concentration in the prepolymerized solution are the main factors in determining the MIP stiffness.[42] Initially, three types of MIP differing in the amount of EGDMA were fabricated, among which the more promising one (based on the frequency shift for a low-concentration solution) was selected for this study. As a rule of thumb, one has to make sure to have a high degree of cross-linker (a minimum of 90 mol % relative to MAA) with moderate wettability, which is vital to stabilize the recognition sites and harvest an acceptable binding affinity.[43] Then, the templates were removed and whether the exertion of electric field would have affected the results was studied, which would exhibit itself in the detection time and the final frequency shift of the EFAMIP-based QCM.

2. MATERIALS AND METHODS

2.1. Materials. 2,2-Azobis(2-isobutyronitrile) (AIBN), ethylene glycol dimethacrylate (EGDMA), methacrylic acid (MAA), IgG from human serum, and phosphate-buffered

https://doi.org/10.1021/acsomega.3c09511
ACS Omega 2024, 9, 16026−16034

saline (PBS) were purchased from Sigma-Aldrich (Milwaukee, WI, USA). All analytical-research-grade chemicals were used without further purification.

2.2. Preparation of EFAMIP and EFAMIP-Modified QCM Surface. First, poly(methacrylic acid) (PMAA) was prepared as follows. One milligram of IgG was added to 3 mL of chloroform in a round-bottom flask; additionally, 2 mL of MAA as a functional monomer and 10 mL of EGDMA as the cross-linker were added to the solution, and to eliminate oxygen, the solution was purged with nitrogen gas for 5 min. Next, 2 mg of AIBN as the initiator was added to the solution, and the tubes were sealed. The solution was sonicated for 10 min. Afterward, some prepolymerized solution was poured on the QCM surface and spin-coated at a relatively low speed. Subsequently, the QCM temperature was maintained at 60 °C for 24 h in an N_2 ambient while applying a vertical electric field of around 36 V cm^{-1}. Both upward and downward vertical electric fields were applied for two different samples of QCMs in order to differentiate between the IgG or F_c or F_{ab} landing fragments during polymerization. Ultraviolet−visible (UV−vis) spectral analysis indicated a peak at 280 nm, which is the IgG's absorption peak, implying that there is still IgG on the QCM surface. After cavities were formed on the surface of the QCM, template removal was achieved by washing the surface with the solution of methanol: acetic acid (9:1, v/v) for 5 min; at this point, the 280 nm peak of UV−vis spectrum disappeared, confirming there is no IgG leftover. The QCM surface was then dried at 60 °C under vacuum for 6 h. Additionally, two control samples, a MIP sample without exerting an electric field and a nonimprinted polymer (NIP) sample, i.e., basically a MIP sample without conducting the template-removal process, were prepared to be compared against the EFAMIP to assess its efficiency. It is noted that NIP usually does not consist of template molecules; however, to make sure that the template removal process is the sole difference maker between MIP and NIP, the NIP in this paper has deviated from the conventional NIPs.

2.3. Measurement Setup. AT-cut, gold/chrome quartz crystal microbalances (QCMs) were purchased from Telemark (Milwaukee, WI, USA), with a nominal 5.983 MHz oscillation frequency and a 13.97 ± 0.03 mm diameter. For measuring the oscillation frequency of QCM, a novel setup was assembled besides the ad hoc-built measurement chamber that was used during the experiment for static measurement in liquids.[44,45] The schematic of the experimental setup is shown in Figure 2a. The ad hoc-built measurement chamber, depicted in Figure 2b, has a small circular slit to expose a specific area of QCM to the liquid. A precise frequency counter (GW, Instek, AFG 2125), being capable of capturing one frequency sample per second with less than 0.1 Hz error, was employed to enhance the recorded frequency data through the experiment. A simple Colpitts oscillating circuit was first improved in regards to its stability and then was used for generating a durable and precise signal for the QCM oscillation frequency. This signal was input to the frequency counter and then the measured frequency was transmitted to a PC for recording.

2.4. Electric Field Setup. As mentioned, the vertical electric field forces the IgG proteins—which act like dipoles in an intermediary buffer pH level condition with little to no impurities—to polarize along the same direction.[37,38] To apply a vertical electric field to the QCM surface and the solution above it, a polished copper plate was placed on top of the ad hoc-built measurement chamber, being parallel with the QCM upper surface (Figure 2a). By applying a voltage bias between the two parallel plates, the desired vertical electric field was generated. To further analyze the protein-binding sites on the MIP surface, two versions of EFAMIP, differing in the direction of the applied electric field, were fabricated. The upward or downward electric field causes the F_c fragments to be closer or farther from the QCM surface, respectively, and makes it oriented.[46,47] In the cases of stagnant or slow flow on the QCM surface, the overall polarization of dipoles should remain the same based on the fact that the net applied forces to the dipole is zero.[48] However, as the solution on the QCM surface becomes stagnant, particles such as proteins start being deposited on the surface.

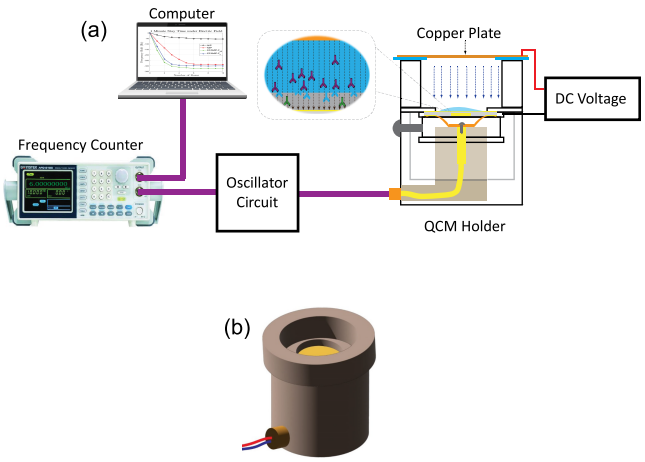

Figure 2. (a) Schematic of the setup that was assembled for the measurement of QCM frequency shift. (b) 3D model of the ad hoc-built measurement chamber. (The frequency counter image source is Farnell.com. Copyright 2024.)

2.5. Characterization Methods. Images of MIPs, i.e., QCM surface, were taken using a scanning electron microscopy system (SEM, TESCAN, VEGA, MV2300/40VP) with an acceleration voltage of about 15 kV. For the assessment of IgG presence, UV−vis spectral analysis (t90+ spectrophotometer, PG Instruments, United Kingdom) was performed both before and after template removal.

3. RESULTS AND DISCUSSION

3.1. Characterization of MIP-Modified QCM Surface. Figure 3 schematically shows the steps followed during the polymerization process. The prepolymerized solution, in which the IgG molecules were randomly oriented, was poured onto the QCM surface (I). By applying a downward electric field, the IgG dipole molecules were aligned so that their F_c fragments were positioned away from the QCM surface (II). The polymerization was initiated (III). Template removal created cavities with orientations paralleling IgG dipole molecules (IV). The EFAMIP-modified QCM surface is ready for detection (V).

The SEM images of the MIPs and the NIP surfaces are shown in Figure 4. Despite being hard to pinpoint individual cavities formed inside the polymer, it is obvious that the NIP surface is much smoother than MIP surfaces wherein there are many pores resulting from IgG template removal.

3.2. Target Detection with MIP-Modified QCM. To ensure that the entropic forces of diffusion, which culminate in a stochastic orientation of target molecules approaching the MIP cavities, were inhibited as much as possible, a static

https://doi.org/10.1021/acsomega.3c09511
ACS Omega 2024, 9, 16026−16034

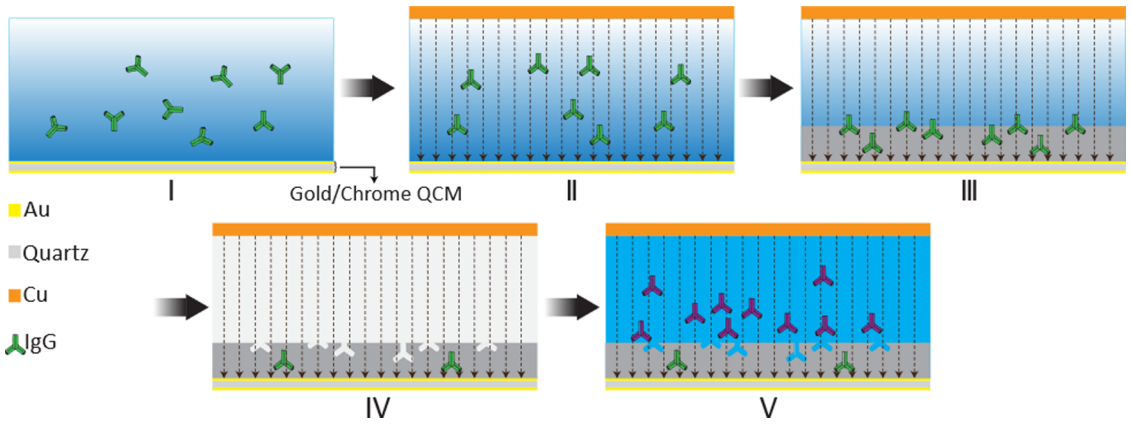

Figure 3. Schematic of the steps used for the fabrication of EFAMIP on a QCM surface: (I) pouring the solution including IgG molecules on the QCM surface prior to polymerization, (II) effect of the applied electric field which forces IgG molecules to be reoriented and aligned with the field, (III) beginning of MAA polymerization, (IV) template removal, and (V) adding fresh IgG solution for rebinding with the cavities formed inside the MIP.

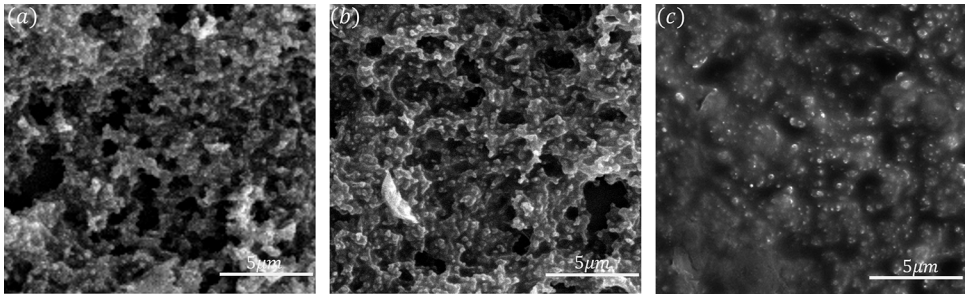

Figure 4. SEM images of (a) typical MIP surface, (b) EFAMIP surface synthesized while exerting an electric field, and (c) NIP surface.

measurement in the liquid phase was planned for assessing the MIP functionality. To begin with, a MIP-modified QCM was placed in an ad hoc-built chamber. At this point, the initial oscillating frequency of the QCM was recorded, typically having a value close to the nominal oscillating frequency. By using a micropipet, 50 μL of deionized water was poured on the QCM. The perturbation from pouring the liquid on the QCM ceased the oscillation of the QCM due to the unstable mass attached to the crystal, resulting in a 0 Hz response for the oscillating frequency. A Colpitts oscillator is highly sensitive to conductance changes in the resonating crystal. Therefore, when the resonator is in contact with a conductive solution, the effective equivalent conductance of the resonator changes, which in turn renders the Colpitts circuit ineffective. This will lead to no signal being generated, hence explaining the measured zero frequency by the frequency counter. However, after drying out the liquid on top of the QCM, the oscillating frequency resets to its initial value since the rigid film mass on top is the same. The drying process was facilitated by removing most of the liquid with a syringe while ensuring that the syringe did not touch the QCM directly. This experiment confirms that the rigid film mass on the QCM determines its oscillating frequency.

Next, to investigate the effect of measurement dynamics on the MIP efficiency, a solution with a concentration of 10 ng/mL IgG in PBS was prepared. In the first approach, 10 μL of this solution was poured on the QCM (for easier referencing, this amount of the solution is referred to as a dose henceforth) and allowed to stay there for 1 min (this time is called the stay time), and after the stay time was over, 50 μL of deionized water was added to the solution above the QCM and agitated slightly. Then, the solution was removed as much as possible with a syringe to ensure that the amount of residual IgG molecules above the QCM was negligible, and the QCM was left untouched until the first stable frequency was recorded. This same process was repeated several times to evaluate the QCM response when exposed to new doses of IgG. The QCM was exposed to new doses until changes in the frequency were very little. A similar experiment with 3 and 5 min stay times was conducted. By performing this characterization, the effect of the IgG solution stay time above the QCM was assessed. An EFAMIP (built with F_{ab} fragments directed toward the QCM surface), a typical MIP, and a NIP underwent this characterization. The frequency shift results are illustrated in Figure 5a. It is obvious that the stay time is directly proportional to the frequency shift simply because a longer time allows a larger number of target molecules to rebind and hence increase the effective mass accumulated on top of the QCM.

In the second approach, the stay time was fixed at 2 min. At the end of each cycle, by pouring 20 μL of methanol:acetic acid (9:1, v/v) on the QCM and agitating it gently for 3 min, then removing the solution and pouring 50 μL of deionized water and removing it, rebound target molecules were washed away to reset the oscillation frequency to its initial value. Even though this process is supposed to reset the frequency completely, some discrepancies between the initial and final frequency values were observed. The result of this approach is depicted in Figure 5b. As evident from the graphs in Figure 5, MIP and EFAMIP displayed slight differences in the frequency shift when being tested under the same conditions, i.e., with no electric field present during the detection phase. It is worth mentioning that the MIP, EFAMIP, and NIP samples that

https://doi.org/10.1021/acsomega.3c09511
ACS Omega 2024, 9, 16026−16034

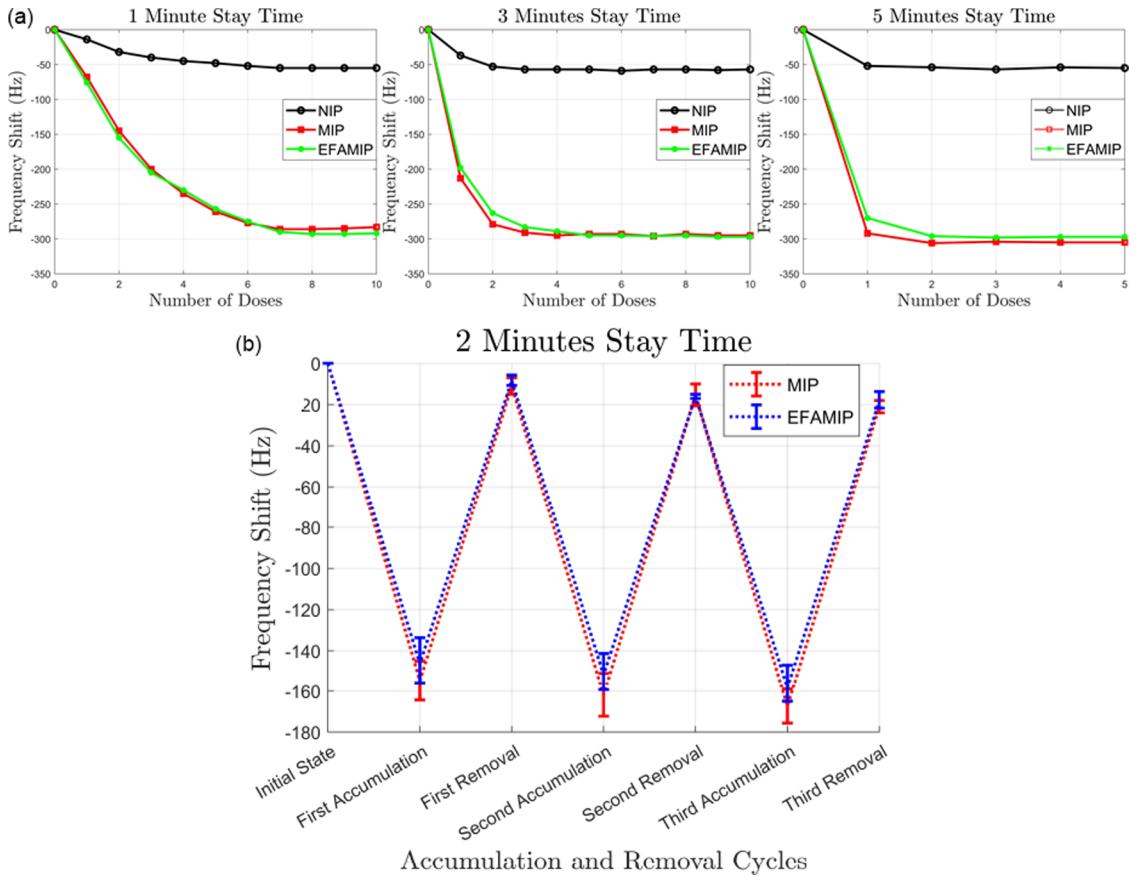

Figure 5. (a) QCM frequency shift vs the number of IgG doses poured on top of the QCM for different stay times. (b) QCM frequency shift through a periodic sequence of detection and removal process (n = 3).

were used in the first approach were replaced with another set in the second approach to ensure that defects or filled cavities do not affect the results.

In the following section, further studies of the MIP-modified QCM were performed by exerting an electric field during the detection phase.

3.3. Enhanced Results Achieved by Applying Electric Field. Using the adjusted ad hoc-built measurement chamber, an electric field was applied to the liquid filled above the QCM during the detection phase. For determining the EFAMIP efficiency, two EFAMIP samples, one with IgG molecules whose F_c fragments directed toward the QCM surface, i.e., EFAMIP-F_c, and another with IgG molecules whose F_{ab} fragments directed toward the QCM surface, i.e., EFAMIP-F_{ab}, were fabricated. While applying a vertical electric field of around 36 V cm^{-1}, along the same direction that was applied through the fabrication process, to the liquid above the QCM, a similar strategy as the first approach in the previous section with 1 min stay time was followed, and the results are shown in Figure 6.

The exertion of an electric field profoundly improved the frequency shifts of both EFAMIP-F_{ab} and EFAMIP-F_c samples while just slightly changing the typical MIP performance. The EFAMIPs exhibited up to 12.5% improvement in their final frequency shift compared to the typical MIP. Obviously, their frequency shifts for the first few doses of IgG improved significantly, which means that the required time for an accurate detection of IgG in a solution is reduced, and the real-time detection is feasible if a proper setup is developed. Being compared against MIP, the EFAMIPs showed up to 113.5%

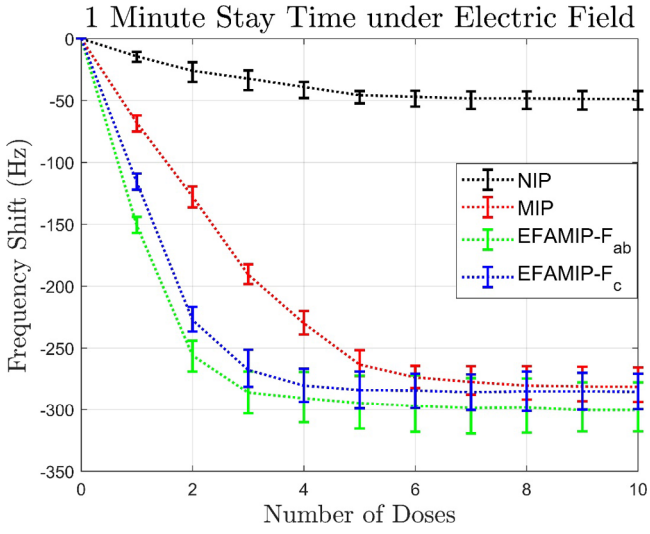

Figure 6. QCM frequency shift in the presence of a vertical electric field vs the number of IgG doses dispensed on top of the QCM (n = 3).

larger frequency shift when the first dose of IgG dispensed. Comparing with the results presented earlier, the sole exertion of the electric field improved the final frequency shift of EFAMIP-F_{ab} by around 10.6%, and the frequency shift in the first few doses was improved by 107.9%. Last, there is not a noticeable change in the NIP-modified QCM frequency shift with the field being present. The comparison of EFAMIP and

https://doi.org/10.1021/acsomega.3c09511
ACS Omega 2024, 9, 16026−16034

MIP for a 1 min stay time under the electric field gives a normalized time constant ratio of 0.369, which highlights the superiority of EFAMIP over MIP.

Indeed, the nonspecific adsorption of IgG and even PBS can result in a slight but incorrect oscillation frequency shift. However, it can be asserted that the ratio of selective bonding to nonspecific adsorption was massive due to the trend in the captured frequency shift data. In fact, the frequency shift versus the analyte concentration captured for NIP demonstrates the nonspecific adsorption of the molecules onto the polymer surface, which clearly shows a distinct separation from the MIP data. Besides, assuming the linear trend to continue for lower concentrations, it can be deduced that this separation is large enough for lower concentrations of IgG to preserve a decent signal-to-noise ratio. Furthermore, the sequential rinsing at the end of each measurement cycle (before the oscillation frequency was captured) was supposed to decrease the error caused by the nonspecific adsorption of target molecules

3.4. EFAMIP and MIP Characterization. Eq 3 exhibits the possible process of identifying the target analyte (IgG) through its interaction with the MIP binding sites:

$$\mathrm{MIP}_{\text{binding site}} + \mathrm{Analyte}_{\text{solution}} \rightleftharpoons \mathrm{Complex}_{\text{analyte-MIP}} \quad (3)$$

Eq 4 defines the association constant K_a in such a system when it reaches equilibrium, where $C_{Complex}$ is the concentration of the refilled binding sites, $C_{Analyte}$ is the analyte concentration, and C_{MIP} is the number of unoccupied binding sites after equilibrium:

$$K_a = \frac{[C_{Complex}]}{[C_{Analyte}][C_{MIP}]} \quad (4)$$

Furthermore, K_a can be extracted from eq 5 that resulted from combining the Langmuir adsorption isotherm and the Sauerbrey equation, in which ΔF_{max} stands for the maximum frequency shift:

$$\Delta F = -\left(\frac{1}{K_a}\right)\frac{\Delta F}{C_{Analyte}} + \Delta F_{max} \quad (5)$$

In order to relatively compare the limit of detection (LOD) and K_a of MIP and EFAMIP, a method similar to the first approach, with a 10 min stay time under an electric field and with a lower dose concentration, was performed. The experiment was repeated three times (n = 3), while at the end of each experiment, target removal was conducted for both MIP and EFAMIP. It is expected for MIP and EFAMIP to have reasonably similar association constants since the EFAMIP solely improved the response time of the sensor, and the equilibrium response of both EFAMIP and MIP was nearly the same. The frequency shifts resulting from this experiment are depicted in Figure 7a. Note that the slopes of the curves in Figure 7a are proportional to $\Delta F_{max}K_a$ (only valid for low concentrations), where for both MIP and EFAMIP, similar association constants are obtained.

As shown in Figure 7a, both EFAMIP and MIP showed reasonably higher association constants compared to NIP, which can be interpreted as a higher selectivity to target molecules. Since the polymerization method was similar for both MIP and EFAMIP, except for the exertion of an electric field, the fabricated polymers atop QCM should be similar in basic properties such as association constants and LOD. Therefore, the final frequency shift or binding constant

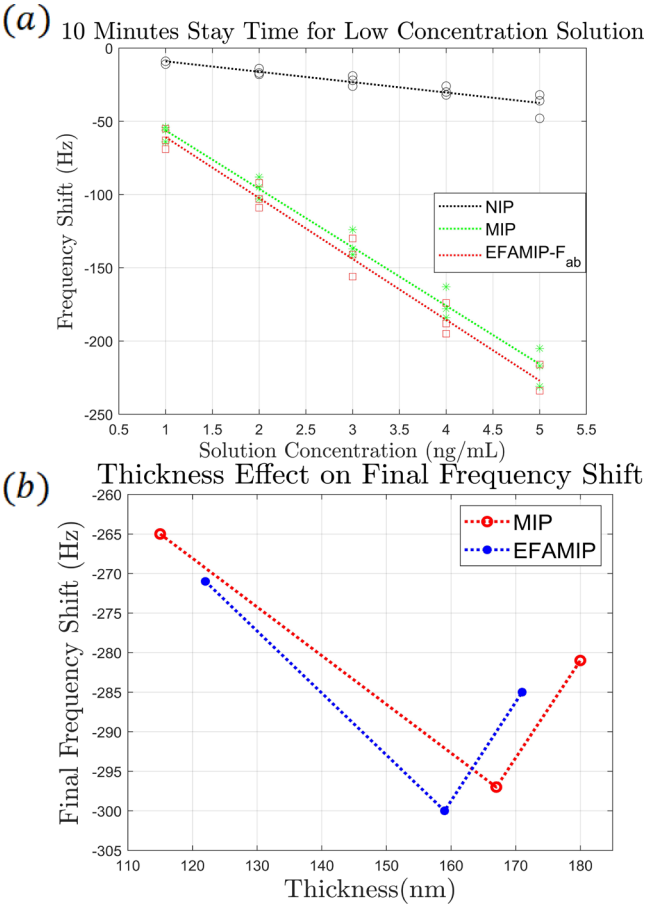

Figure 7. (a) QCM frequency shift for low concentrations of IgG in the presence of a vertical electric field with a long stay time, i.e., after reaching equilibrium. (b) Final frequency shift vs thickness for MIP and EFAMIP.

achieved should be similar for both MIP and EFAMIP. However, the dynamic response of EFAMIP was raised above MIP, which consequently resulted in a faster time response of the sensor.

The thickness of MIP plays an important role in the efficiency of its binding performance. If the MIP layer is too thick, more IgG molecules will be buried inside the polymer, rendering the elution procedure less effective in removing the molecules beneath the surface.[49] On the other hand, due to the porosity of the MIP layer, if the layer is too thin, securing the homogeneity will not be possible. SEM images of the MIP layer are often considered as a reliable indication of the homogeneity of the imprinted polymer.[50] The SEM images of this paper, as that of other papers,[51,52] suggest a homogeneous layer of MIP. Also, research shows that oriented immobilization of the protein molecules effectively reduces inhomogeneity.[52] The electric field we applied to MIP plays the role of an oriented immobilizer in this research.[39]

In order to analyze the effect of the thickness of the polymer on the performance of the sensor, three MIP and EFAMIP samples with various thicknesses were prepared. Using a similar approach as pointed out in Section 3.3, the final frequency shift of these samples was measured. Three MIP samples with thicknesses of 115, 167, and 180 nm had corresponding final frequency shift values of −265, −297, and −281 Hz, respectively. EFAMIP samples with thicknesses of 122, 159, and 171 nm had the corresponding final frequency

https://doi.org/10.1021/acsomega.3c09511
ACS Omega 2024, 9, 16026−16034

shift values of −271, −300, and −285 Hz, respectively. Figure 7b depicts the measured frequency shift for each thickness. The acquired data pinpoint a local maximum in the frequency shift of both MIP and EFAMIP around 165 nm. Furthermore, EFAMIP and MIP appear to have the same relation with respect to the thickness.

Additionally, the MIP stability was studied. The MIP samples only showed a 3.3% reduction in the final frequency shift after being left in ambient conditions for 3 weeks, making this method a promising approach to a low-cost and reliable diagnosis procedure.

4. DISCUSSION

As seen in Figure 6, EFAMIP-F_{ab} performed slightly better than EFAMIP-F_c based on their final frequency shift. This might be primarily due to the unique structure of this fragment, which, during the polymerization process, can create more distinctive cavities. In any case, since the F_{ab} fragments, referred to as antigen-binding sites[53] are the major difference among different antibodies, EFAMIP-F_{ab} is expected to outperform the MIPs in actual sensing applications. It is anticipated to perform well even if the solution contains different types of antibodies because the electric field can force the immunoglobulins to approach EFAMIP with their F_{ab} fragments, culminating in a more selective binding process. This characteristic of EFAMIP-F_{ab} can make it a feasible commercial biosensor for the early and fast detection of infections. Following the same logic, solutions containing limited dipolar molecules suit the EFAMIP. Other immunoglobins or proteins that show a strong or moderate dipole effect can also be utilized to create EFAMIP. Most antibody molecules have a Y shape, which results in a nonbalanced electron distribution and, consequently, a nonzero dipole moment. Therefore, IgG molecules are only used for the proof-of-concept, and there is room to study other molecules in the suggested EFAMIP setup. In fact, any protein that can undergo a global rearrangement of dipole moments at the amide planes under an electric field, which in turn may impair hydrogen-bond stability, is suitable for the EFAMIP.

Further investigation of the electric field direction and amplitude can arise. For instance, a lateral electric field can be applied to tilt the target molecules during the polymerization and detection process. This method might be more beneficial for dynamic measurement in liquid since the target molecules move along the flow above the QCM during the detection phase. For example, studies that rely on a microfluidic channel to bring the target molecules onto the QCM might benefit more from a diagonal or lateral electric field. In this strategy, the direction of electric field is wisely adjusted by including all other forces to reorient the target molecules along a direction paralleling the exact same direction of the cavities formed during the polymerization. This scheme can inhibit the long response time that dynamic measurements in liquid suffer from and might also improve the detection limit.

5. CONCLUSIONS

In this report, by revisiting the MIP preparation and examination process, EFAMIP as an enhanced form of MIP was fabricated. The EFAMIP was proved to be a promising way of boosting the performance of MIP-modified QCM sensors for detecting dipolar complex molecules. The fabricated EFAMIP-modified QCM also reduced the required time to sense target molecules in samples, which consequently can speed up the diagnostics. The EFAMIPs showed up to 113.5% more frequency shift than typical MIP while being in contact with IgG. The EFAMIP final frequency shift was also improved by 10.6% when applying an electric field. Furthermore, EFAMIP-F_{ab} exhibited remarkable capability for antibody detection, especially in solutions containing various types of immunoglobulins. Finally, the method presented here is very useful for samples that contain a limited number of dipolar molecules since the electric field can only affect the dipole molecule orientation.

AUTHOR INFORMATION

Corresponding Author

Majid Badieirostami − *MEMS Lab, School of Electrical and Computer Engineering, College of Engineering, University of Tehran, Tehran 1439957131, Iran;* orcid.org/0000-0002-1647-7052; Email: mbadiei@ut.ac.ir

Authors

Iliya LariMojarad − *MEMS Lab, School of Electrical and Computer Engineering, College of Engineering, University of Tehran, Tehran 1439957131, Iran;* orcid.org/0009-0004-7866-2861

MirBehrad Mousavi − *MEMS Lab, School of Electrical and Computer Engineering, College of Engineering, University of Tehran, Tehran 1439957131, Iran*

Mohammad Mahdi Moeini Manesh − *MEMS Lab, School of Electrical and Computer Engineering, College of Engineering, University of Tehran, Tehran 1439957131, Iran*

Mohammadjavad Bouloorchi Tabalvandani − *MEMS Lab, School of Electrical and Computer Engineering, College of Engineering, University of Tehran, Tehran 1439957131, Iran;* orcid.org/0009-0007-5539-3074

Complete contact information is available at: https://pubs.acs.org/10.1021/acsomega.3c09511

Notes

The authors declare no competing financial interest.

ACKNOWLEDGMENTS

The authors would like to acknowledge Hamed Abadijoo, Seyed Ahmadreza Firoozabadi, Saeed Javadizadeh, and Zahra Saeidpour from MEMS Lab for their help and support.

REFERENCES

(1) Mohankumar, P.; Ajayan, J.; Mohanraj, T.; Yasodharan, R. Recent developments in biosensors for healthcare and biomedical applications: A review. *Measurement* **2021**, *167*, No. 108293.

(2) Selvolini, G.; Marrazza, G. MIP-Based Sensors: Promising New Tools for Cancer Biomarker Determination. *Sensors* **2017**, *17* (4), 718.

(3) Parihar, A.; Ranjan, P.; Sanghi, S. K.; Srivastava, A. K.; Khan, R. Point-of-Care Biosensor-Based Diagnosis of COVID-19 Holds Promise to Combat Current and Future Pandemics. *ACS Appl. Bio Mater* **2020**, *3* (11), 7326−7343.

(4) Zamani, M.; Furst, A. L.; Klapperich, C. M. Strategies for engineering affordable technologies for point-of-care diagnostics of infectious diseases. *Acc. Chem. Res.* **2021**, *54* (20), 3772−3779.

(5) Justino, C. I.; Duarte, A. C.; Rocha-Santos, T. A. Recent progress in biosensors for environmental monitoring: A review. *Sensors* **2017**, *17* (12), 2918.

(6) Tai, D. F.; Jhang, M. H.; Chen, G. Y.; Wang, S. C.; Lu, K. H.; Lee, Y. D.; Liu, H. T. Epitope-cavities generated by molecularly

https://doi.org/10.1021/acsomega.3c09511
ACS Omega 2024, 9, 16026−16034

imprinted films measure the coincident response to anthrax protective antigen and its segments. *Anal. Chem.* **2010**, *8* (6), 2290−2293.
(7) Fatima, A.; Younas, I.; Ali, M. W. An Overview on Recent Advances in Biosensor Technology and Its Future Application. *Arch. Pharm. Pract.* **2022**, *13* (1), 5−10.
(8) Anirudhan, T. S.; Rejeena, S. R. Poly(methacrylic acid-co-vinyl sulfonic acid)-grafted-magnetite/nanocellulose superabsorbent composite for the selective recovery and separation of immunoglobulin from aqueous solutions. *Sep. Purif. Technol.* **2013**, *119*, 82−93.
(9) Haupt, K.; Medina Rangel, P. X.; Bui, B. T. S. Molecularly Imprinted Polymers: Antibody Mimics for Bioimaging and Therapy. *Chem. Rev.* **2020**, *120* (17), 9554−9582.
(10) Raziq, A.; Kidakova, A.; Boroznjak, R.; Reut, J.; Öpik, A.; Syritski, V. Development of a Portable MIP-Based Electrochemical Sensor for Detection of SARS-CoV-2 Antigen. *Biosens. Bioelectron.* **2021**, *178*, No. 113029.
(11) Goldberg, R. J. A Theory of Antibody—Antigen Reactions. I. Theory for Reactions of Multivalent Antigen with Bivalent and Univalent Antibody2. *J. Am. Chem. Soc.* **1952**, *74* (22), 5715−5725.
(12) Forthal, D. N. Functions of Antibodies. *Microbiol. Spectr.* **2014**, *2* (4), 1.
(13) Vidarsson, G.; Dekkers, G.; Rispens, T. IgG subclasses and allotypes: from structure to effector functions. *Front. Immunol.* **2014**, *5*, 520.
(14) Kandori, K.; Miyagawa, K.; Ishikawa, T. Adsorption of immunogamma globulin onto various synthetic calcium hydroxyapatite particles. *J. Colloid Interface Sci.* **2004**, *273* (2), 406−413.
(15) Guha, A.; Ahmad, O. S.; Guerreiro, A.; Karim, K.; Sandström, N.; Ostanin, V. P.; van der Wijngaart, W.; Piletsky, S. A.; Ghosh, S. K. Direct Detection of Small Molecules Using a Nano-Molecular Imprinted Polymer Receptor and a Quartz Crystal Resonator Driven at a Fixed Frequency and Amplitude. *Biosens. Bioelectron.* **2020**, *158*, No. 112176.
(16) Chrzanowska, A. M.; Poliwoda, A.; Wieczorek, P. P. Characterization of particle morphology of biochanin A molecularly imprinted polymers and their properties as a potential sorbent for solid-phase extraction. *Mater. Sci. Eng. C,* **2015**, *49*, 793−798.
(17) Viveiros, R.; Rebocho, S.; Casimiro, T. Green Strategies for Molecularly Imprinted Polymer Development. *Polymers* **2018**, *10* (3), 306.
(18) Srivastava, J.; Singh, R. S.; Singh, M. Design of EQCM-MIP Sensing Matrix for Highly Specific and Sensitive Detection of Thyroglobulin. *Biosens. Bioelectron. X* **2022**, *11*, No. 100154.
(19) Prabakaran, K.; Jandas, P. J.; Luo, J.; Fu, C.; Wei, Q. Molecularly imprinted poly (methacrylic acid) based QCM biosensor for selective determination of L-tryptophan. *Colloids Surf., A* **2021**, *611*, No. 125859.
(20) Aylaz, G.; Andaç, M.; Denizli, A.; Duman, M. Recognition of human hemoglobin with macromolecularly imprinted polymeric nanoparticles using non-covalent interactions. *J. Mol. Recogn.* **2021**, *34* (12), No. e2935.
(21) Pesavento, M.; Marchetti, S.; De Maria, L.; Zeni, L.; Cennamo, N. Sensing by Molecularly Imprinted Polymer: Evaluation of the Binding Properties with Different Techniques. *Sensors* **2019**, *19* (6), 1344.
(22) Cui, Y.; Ding, J.; Su, Y.; Ding, L. Facile Construction of Magnetic Hydrophilic Molecularly Imprinted Polymers with Enhanced Selectivity Based on Dynamic Non-Covalent Bonds for Detecting Tetracycline. *Chem. Eng. J.* **2023**, *452*, No. 139291.
(23) Advincula, R. C. Engineering molecularly imprinted polymer (MIP) materials: Developments and challenges for sensing and separation technologies. *Korean J. Chem. Eng.* **2011**, *28*, 1313−1321.
(24) Alassi, A.; Benammar, M.; Brett, D. Quartz Crystal Microbalance Electronic Interfacing Systems: A Review. *Sensors* **2017**, *17* (12), 2799.
(25) Haghdoust, S.; Arshad, U.; Mujahid, A.; Schranzhofer, L.; Lieberzeit, P. A. Development of a MIP-Based QCM Sensor for Selective Detection of Penicillins in Aqueous Media. *Chemosensors* **2021**, *9* (12), 362.
(26) Whitcombe, M. J.; Chianella, I.; Larcombe, L.; Piletsky, S. A.; Noble, J.; Porter, R.; Horgan, A. The rational development of molecularly imprinted polymer-based sensors for protein detection. *Chem. Soc. Rev.* **2011**, *40* (3), 1547−1571.
(27) Akgönüllü, S.; Kılıç, S.; Esen, C.; Denizli, A. Molecularly Imprinted Polymer-Based Sensors for Protein Detection. *Polymers* **2023**, *15* (3), 629.
(28) Wisnu, A. A.; Dobler, M. T.; Lieberzeit, P. A. QCM-Based Assay Designs for Human Serum Albumin. *Anal. Bioanal. Chem.* **2022**, *414* (1), 731−741.
(29) Lim, H. J.; Saha, T.; Tey, B. T.; Lal, S. K.; Ooi, C. W. Quartz Crystal Microbalance-Based Biosensing of Proteins Using Molecularly Imprinted Polydopamine Sensing Films: Interplay between Protein Characteristics and Molecular Imprinting Effect. *Surf. Interfaces* **2023**, *39*, No. 102904.
(30) Park, R.; Jeon, S.; Jeong, J.; Park, S.-Y.; Han, D.-W.; Hong, S. W. Recent Advances of Point-of-Care Devices Integrated with Molecularly Imprinted Polymers-Based Biosensors: From Biomolecule Sensing Design to Intraoral Fluid Testing. *Biosensors* **2022**, *12* (3), 136.
(31) Hu, J.; Huang, X.; Xue, S.; Yesilbas, G.; Knoll, A.; Schneider, O. Measurement of the Mass Sensitivity of QCM with Ring Electrodes Using Electrodeposition. *Electrochem. Commun.* **2020**, *116*, No. 106744.
(32) Setiana, M.; Zafirah, T. N.; Masruroh; Istiroyah; Satki, S. P. Impedance Spectrum of QCM Sensor Coated with 18-Crown-6-Ether Solved in THF, Chloroform and Toluene. *IOP Conf. Ser.: Mater. Sci. Eng.* **2020**, *833* (1), No. 012091.
(33) Johannsmann, D.; Langhoff, A.; Leppin, C. Studying Soft Interfaces with Shear Waves: Principles and Applications of the Quartz Crystal Microbalance (QCM). *Sensors* **2021**, *21* (10), 3490.
(34) Thies, J. W.; Kuhn, P.; Thürmann, B.; Dübel, S.; Dietzel, A. Microfluidic quartz-crystal-microbalance (QCM) sensors with specialized immunoassays for extended measurement range and improved reusability. *Microelectron. Eng.* **2017**, *179*, 25−30.
(35) Adel, M.; Allam, A.; Sayour, A. E.; Ragai, H. F.; Umezu, S.; Fath El-Bab, A. M. R. Design and Development of a Portable Low-Cost QCM-Based System for Liquid Biosensing. *Biomed. Microdevices* **2024**, *26* (1), 11.
(36) Zhou, J.; Tsao, H. K.; Sheng, Y. J.; Jiang, S. Monte Carlo simulations of antibody adsorption and orientation on charged surfaces. *J. Chem. Phys.* **2004**, *121* (2), 1050−1057.
(37) Gajos, K.; Awsiuk, K.; Budkowski, A. Controlling Orientation, Conformation, and Biorecognition of Proteins on Silane Monolayers, Conjugate Polymers, and Thermo-Responsive Polymer Brushes: Investigations Using TOF-SIMS and Principal Component Analysis. *Colloid Polym. Sci.* **2021**, *299* (3), 385−405.
(38) Diyya, S. *Influence of electric field on IgG positioning and its immobilization for solid immunosensing substrate*; Europe PMC. https://europepmc.org/article/ppr/ppr628771 (accessed February 2024).
(39) Emaminejad, S.; Javanmard, M.; Gupta, C.; Chang, S.; Davis, R. W.; Howe, R. T. Tunable control of antibody immobilization using electric field. *Proc. Natl. Acad. Sci. U. S. A.* **2015**, *112* (7), 1995−1999.
(40) Kim, H. J.; Park, D.; Park, Y.; Kim, D. H.; Kim, J. Electric-Field-Mediated In-Sensor Alignment of Antibody's Orientation to Enhance the Antibody−Antigen Binding for Ultrahigh Sensitivity Sensors. *Nano Lett.* **2022**, *22* (16), 6537−6544.
(41) Curk, T.; Dobnikar, J.; Frenkel, D. Rational Design of Molecularly Imprinted Polymers. *Soft Matter* **2016**, *12* (1), 35−44.
(42) Wulff, G. Molecular Imprinting in Crosslinked Polymers - the Role of the Binding Sites. *Mol. Cryst. Liq. Cryst. Sci. Technol., Sect. A* **1996**, *276* (1−2), 1−6.
(43) Pardo, A.; Mespouille, L.; Dubois, P.; Blankert, B.; Duez, P. Molecularly Imprinted Polymers: Compromise between Flexibility and Rigidity for Improving Capture of Template Analogues. *Chem.—Eur. J.* **2014**, *20* (12), 3500−3509.
(44) Fort, A.; Panzardi, E.; Vignoli, V.; Tani, M.; Landi, E.; Mugnaini, M.; Vaccarella, P. An adaptive measurement system for the

https://doi.org/10.1021/acsomega.3c09511
ACS Omega 2024, 9, 16026−16034

simultaneous evaluation of frequency shift and series resistance of QCM in liquid. *Sensors* **2021**, *21* (3), 678.
(45) Addabbo, T.; Fort, A.; Landi, E.; Moretti, R.; Mugnaini, M.; Vignoli, V. Strategies for the accurate measurement of the resonance frequency in QCM-D systems via low-cost digital techniques. *Sensors* **2022**, *22* (15), 5728.
(46) Lou, D.; Ji, L.; Fan, L.; Ji, Y.; Gu, N.; Zhang, Y. Antibody-Oriented Strategy and Mechanism for the Preparation of Fluorescent Nanoprobes for Fast and Sensitive Immunodetection. *Langmuir* **2019**, *35* (14), 4860−4867.
(47) Ghisellini, P.; Caiazzo, M.; Alessandrini, A.; Eggenhöffner, R.; Vassalli, M.; Facci, P. Direct Electrical Control of IgG Conformation and Functional Activity at Surfaces. *Sci. Rep.* **2016**, *6* (1), 37779.
(48) Serway, R. A.; Jewett, J. W. *Physics for Scientists and Engineers with Modern Physics*, 10th ed.; Cengage Learning: Boston, 2018.
(49) Dong, C.; Shi, H.; Han, Y.; Yang, Y.; Wang, R.; Men, J. Molecularly Imprinted Polymers by the Surface Imprinting Technique. *Eur. Polym. J.* **2021**, *145*, No. 110231.
(50) Akgönüllü, S.; Battal, D.; Yalcin, M. S.; Yavuz, H.; Denizli, A. Rapid and Sensitive Detection of Synthetic Cannabinoids JWH-018, JWH-073 and Their Metabolites Using Molecularly Imprinted Polymer-Coated QCM Nanosensor in Artificial Saliva. *Microchem. J.* **2020**, *153*, No. 104454.
(51) Castro-Grijalba, A.; Montes-García, V.; Cordero-Ferradás, M. J.; Coronado, E.; Pérez-Juste, J.; Pastoriza-Santos, I. SERS-Based Molecularly Imprinted Plasmonic Sensor for Highly Sensitive PAH Detection. *ACS Sens.* **2020**, *5* (3), 693−702.
(52) Liu, L.; Zheng, J.; Fang, G.; Xie, W. Improvement of the Homogeneity of Protein-Imprinted Polymer Films by Orientated Immobilization of the Template. *Anal. Chim. Acta* **2012**, *726*, 85−92.
(53) Raghunathan, G.; Smart, J.; Williams, J.; Almagro, J. C. Antigen-Binding Site Anatomy and Somatic Mutations in Antibodies That Recognize Different Types of Antigens. *J. Mol. Recognit.* **2012**, *25* (3), 103−113.

https://doi.org/10.1021/acsomega.3c09511
ACS Omega 2024, 9, 16026−16034